Hindawi
International Journal of Photoenergy
Volume 2023, Article ID 2620367, 13 pages
https://doi.org/10.1155/2023/2620367

Research Article

Implementation of Modified SEPIC Converter for Renewable Energy Built DC Microgrids

B. Jyothi,[1] P. Bhavana,[2] B. Thirumala Rao,[3] Mukesh Pushkarna,[4] Kitmo ,[5] and Repele Djidimbele [5]

[1]*EEE Department, Koneru Lakshmaiah Education Foundation, Vaddeswaram, Guntur, India*
[2]*EEE Department, SRKIT, Vijayawada, India*
[3]*EEE Department, Sri Venkateswara College of Engineering and Technology, RVS Nagar, Chittoor, India*
[4]*Department of Electrical Engineering, GLA University Mathura, Mathura, India*
[5]*Department of Renewable Energy, National Advanced School of Engineering of Maroua, University of Maroua, Cameroon*

Correspondence should be addressed to Repele Djidimbele; repele2021@gmail.com

Received 9 September 2022; Revised 8 March 2023; Accepted 16 March 2023; Published 30 March 2023

Academic Editor: Elias Stathatos

The nonavailability of fossil fuels and the shortcomings of nonconventional energy sources taking place in the environment lead the research and development towards alternative and clean energy sources such as renewable energy sources. Renewable or nonconventional energy resources are being used to meet ever-increasing energy demand. The photo voltaic (PV) energy is the right choice of renewable energy for small voltage DC distribution systems, due to their advantages. But this energy source can produce low output power at the utility grid. Hence, to step up this low input voltage to high value for a range of high-voltage applications, DC-DC converters are integrated to the DC microgrids by means of PV system. The present work elaborates the modified SEPIC converter (MSC) designed based on the traditional SEPIC with a boost-up module. In comparison with conventional or traditional SEPIC converter, the proposed MSC produces high voltage gain and continuous current to the DC microgrids. Furthermore, MSC is operated with only one controlled switch. The proposed converter design improves the efficiency, output voltage, and continuous output current of the DC microgrids. This entire work is completed with PSIM, and finally, numerical simulation results prove the possibility of the MSC with PV-powered DC microgrids, and also the dynamic response of MSC for DC microgrid loads enhances the regulated output voltage and continuous output current of DC loads.

1. Introduction

Nonconventional energy sources are biomass, tidal, and geothermal energy sources that exist in nature in particular regional sectors. But solar and wind energies are abundant in nature and available in all regional sectors. Especially, solar and wind energy sources give maximum efficiency and reliability when compared with other nonconventional energy sources. Moreover, the upcoming research focuses on these two renewable energy sectors integrated to the AC and DC grids [1–3].

Normally, in the perception of the microgrid, DC microgrids are implemented easily due to the availability of distributed energy sources like nonconventional energy sources (PV cells and fuel cells), energy storing devices like batteries, supercapacitors, etc. can store electrical energy in the form of DC. Hereafter, research is focused towards the implementation of DC microgrids with PV cells, batteries, etc. for satisfying the DC load demand. The deficiency of electricity is one of the main obstacles in the development of rural India. Hence, in the present Indian scenario, stand-alone solar systems are gaining much attention, and they are becoming a very competitive solution, particularly because of the availability of more sunny days throughout the year. One such essential application of PV standalone system is supplying rural areas in efficient way. In India after 2010, DC microgrids are popular with the renewable energy integration for satisfying DC loads in commercial and

residential areas. In the case of DC microgrids, solar photovoltaic systems, fuel cells, etc. require the DC supply sources. Out of many renewable energy sources, solar PV systems are low cost, nonpollutant, free available source, and ecofriendly to the environment [1].

Another important feature regarding the DC microgrid is one can easily implement with one or two DC-DC converters, but AC microgrids require a larger number of both DC-DC and DC-AC converters. As a result, DC microgrids required less expensive materials, and also, these grids provide an improved efficiency compared with the AC microgrids. In DC, microgrids are very simple to operate due to the absence of frequency, harmonic distortion and reactive power, and no grid synchronization with the network. In the case of AC microgrids, synchronization of the grid plays a major role. Designing a control structure for DC microgrids is simple w.r.t AC microgrids [4–6].

The proposed work is focused on the application of DC microgrids with DC-DC converters for effective driving of the DC loads as it is shown in Figure 1. Solar energy is preferred as input resource for DC microgrids. PV panel-based solar systems are giving electricity directly from the sunlight, and these PV systems require less space and low cost and give maximum efficiency designed for DC microgrids when compared with the solar thermal collectors. As a result, upcoming research work is carried out on DC microgrids through PV systems to fulfill the DC load demand. The low DC voltage coming from the PV panels cannot drive a high voltage DC applications requirement in DC microgrids.

To enhance the voltage, suitable converters are enabled through PV panel integration, which plays a major role [2]. PV panels allied with DC loads by using isolated or nonisolated DC-DC converters to attain continuous output current and more voltage gain at DC microgrids. By using high frequency (HF) transformer and changing its turn ratio, one can easily get a boost-up voltage at the output side in isolated DC-DC converters [7, 8]. But, it produces voltage ripples, high voltage stress, and leakage currents. Furthermore, very large-size high-frequency transformers are placed in these isolated converters to properly produce an output voltage in the boost module, etc. [9]. But the size of the converter is increased and leads to the bulk in size. Thus, in most of the high-voltage applications, one can prefer nonisolated DC-DC converters rather than the isolated one. In earlier days, traditional nonisolated DC-DC converters are operated with a maximum duty ratio to get high voltage. However, the maximum duty ratio (approximately ranges from 0.85 to 0.95) lowers the efficiency and creates no functionality of the converter. In modern trends, several DC-DC converters to achieve high voltage gain can be used with passive elements [10, 11]. Therefore, a compact size, high efficiency, continuous current etc. are the requirements of economic considerations for DC-DC converters. Several voltage-boosting methods like coupled inductor cascading of converters attaining high output voltage of DC-DC converters with nonisolation are addressed [12–15]. Coupled inductors can control the output voltage based on the inductor coil turns ratio alteration. This coupled inductor leakage inductance produces ripples in the power switch current. To reduce the current spike in the coupled inductor, these converters require a clamping circuit.

In cascaded nonisolated DC-DC converters, the quadratic boost converters (QBC) are the best example to produce output voltage with boosting module in a quadratic manner; however, high voltage stress occurs at power switches and diodes. The high voltage multiplier 2^{nd} order boost nonisolated DC-DC converter is deliberated in [16]. This converter's output voltage is influenced by the number of voltage multipliers and duty ratio. On the other hand, it generates the less magnitude of the output voltage, though this converter is equipped with a number of voltage multipliers. An active network-based switched-capacitor nonisolated DC-DC converter with high gain is presented in [17]. This converter produces higher voltage gain with poor voltage regulation and pulsating current at the load side. But it gives a discontinuous current at the supply side, which is another drawback. Hence, the converter indicates the utilization of the supply sources in minimum [16–19].

The proposed MSC [20] can overcome the problems of conventional nonisolated and isolated DC-DC converters addressed in [7–19]. This converter can simply operate with one switch that diminishes the difficulty in controlling of gate pulses for the switch [11]. Moreover, it provides continuous current at both supply and load sides, more voltage gain, and the utmost utilization of input resources. Furthermore, it has negligible voltage stress across the diode and switch compared with a novel distinct-switch buck-boost DC-DCSEPIC converter. Hence, it is used for integrated PV-based DC microgrid systems to achieve high efficiency, voltage gain, and continuous output current to the utility grids. PV array with maximum power point tracking (MPPT) is a very important part of the PV system. Researchers develop and implement many MPPT techniques used for PV arrays to generate maximum power and transmit that power to the load to meet the load demand [21]. These techniques are varied w.r.t sensors required, complexity, range of effectiveness, convergence speed, etc. Table 1 can be able to describe the merits of the P&O MPPT technique compared with the other MPPT techniques [22].

The DC-DC converter can effectively utilize in transmitting MPP from the PV array to the load. Through regulating the duty cycle of the pulse width modulation control, the DC-DC converter's load voltage differs and obtains the MPP with the input source (PV array) to transmit the maximum power. To increase the efficiency of the PV system with an effective MPPT controller is necessary to maintain the operating point of the PV array at the maximum power point in all ecological situations. Therefore, maintaining an MPPT of the PV array mandatorily requires a better MPPT controller with less convergence time and less complexity in its controller algorithm. For this, researchers developed many MPPT techniques such as perturb and observe (P&O) technique, hill climbing (HC) technique, incremental conductance (IC) technique, etc. But most of the researchers used the P&O MPPT technique, which is quite easy, fewer algorithm steps, and also gives a fast response associated with this MPPT controller rather than the remaining other MPPT techniques [22].

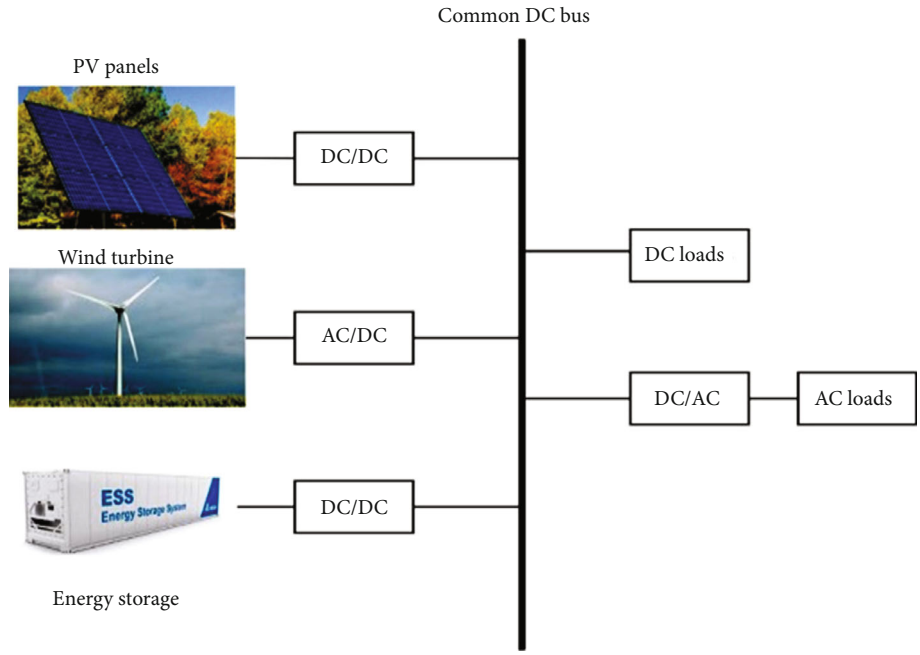

Figure 1: Overview of DC microgrid.

Table 1: Comparison of P&O, incremental conductance MPPT technique.

Parameters	P&O MPPT technique	Incremental conductance MPPT technique
Convergence speed	Varies	Varies
Implementation capacity	Low	High
Sensed parameters	Both current and voltage	Maximum voltage
Response time	Less	More
Analog or digital	Both digital and analog	Only digital
Number of iterations	Less	More

In case the PV system meet the load demand in partially shaded conditions and in rainy days, backup should be provided to them with DC microgrids through the battery by using a bidirectional DC-DC converter [BDC]. This article focuses on the half-bridge BDC due to its performance (voltage gain, switch stress, etc.) [23], when compared with the BDCs [9–24]. Here, the proposed BDC is a nonisolated DC-DC converter, and it requires only two switches with three passive elements (two capacitors and one inductor); moreover, it reduces the cost of the converters. When the system with a battery and PV array is used as input sources to the DC, microgrids can effectively satisfy the DC load demand. If the PV system is fully satisfying the DC microgrid system, then the proposed BDC is operated in buck mode to store the DC voltage in a battery. If the PV system cannot satisfy the DC loads in DC microgrid necessities, their BDC can operate in boost mode and make the battery supply a DC voltage to meet the DC loads with their requirements in DC microgrids.

The main aim of the proposed work is to integrate the MSC with DC microgrids to effectively operate the DC loads which are connected through the DC microgrids. Moreover, the high voltage gain and continuous output current produced by this MSC are some of the key features to drive DC loads in DC microgrids in an efficient way. Hence, the motive of this MSC with less passive elements requirement is well suited for the applications of both renewable energy and DC microgrids.

The paper is organized as follows: section II and III elaborated about the performance analysis of conventional SEPIC converter and MSC. The importance of the half-bridge BDC for the PV system-based DC microgrids is addressed in section IV. Discussions on simulation outcomes of the MSC, the half-bridge BDC, the PV system-based DC microgrid with MSC, and the dynamic response of the overall system are viewed in section V. Conclusion of the proposed work is given in section VI.

2. Conventional SEPIC Converter

Conventional or traditional SEPIC converter is also termed as a single-ended primary inductor converter (SEPIC). In general, it is used in the high-voltage renewable energy

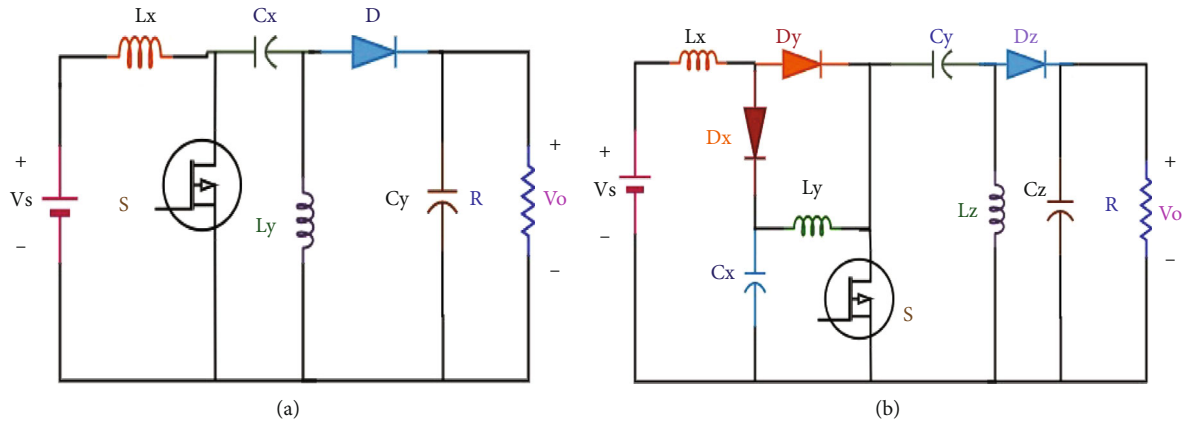

Figure 2: (a) Conventional SEPIC converter and (b) proposed MSC circuit diagram.

applications. But the problem associated with this converter is listed as follows:

(1) It produces less voltage gain

(2) It generates ripples at the output side (load side) when this converter takes input voltage with some noise signals

(3) This converter does not properly utilize input resources in the required manner

The difficulties related with this conventional SEPIC converter are overcome with the MSC discussed in section III. Moreover, conventional SEPIC converter needs extreme duty ratio to operate a converter in a boost mode. Thus, it affects the efficiency and functionality of the system when operated at the maximum duty ratio. But MSC does not need any maximum duty ratio point, and the converter operates in boost mode with a duty ratio of 0.55 to 1 in an efficient manner without producing any unwanted disconcerting signals. The circuit diagram of the conventional SEPIC converter shown in Figure 2 operates like a buck-boost DC-DC converter, but it continuously generates output current.

3. Modified SEPIC Converter

MSC includes input-output terminals and derivatives by changing the conventional SEPIC converter presented in Figure 2. Elaborated operation of the MSC is shown in Figure 2(b) using switch S by means of switching frequency (f_s) with other elements like diodes, inductors, and capacitors. The capacitor C_x and inductor L_y act as the voltage-boosting components by adding a D_x, D_y diodes in MSC. Proposed MSC merits are as follows: (1) MSC operates by a single power switch that decreases the difficulty of controller circuitry. (2) This converter produces input current without any distortions. (3) It gives more gain w.r.t voltage. (4) MSC utilizing the sources effectively on input.

Therefore, MSC-integrated PV system-based DC microgrids are proposed. Few assumptions are considered to evaluate the steady-state operation of the MSC at ideal,

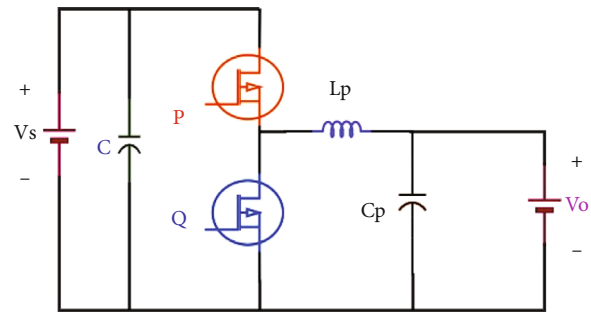

Figure 3: Half-bridge BDC.

and all capacitors are large and sufficient to attain constant voltage. The modified SEPIC converter can operate in 2 modes to obtain the continuous output current as shown in Figures 3 and 4.

3.1. Mode 1 ($t_0 - t_1$). Mode1 3 inductors are attaining the following current path when these inductors are magnetized: inductor current I_{Lx} follows the path from source voltage and showed with a red dotted line path (Figure 5(a), 1A). Second current I_{Ly} flows from capacitor C_x path shown in Figure 5(a)), 1B, and I_{Lz} flows from capacitor C_y, and it follows the path as 2 as shown in Figure 5(a). At this juncture diode D_z is reverse biased by capacitor C_z and transfers the energy to the DC load.

$$V_{Lx} = V_{s,} \tag{1}$$

$$V_{Ly} = V_{Cx,} \tag{2}$$

$$V_{Lz} = V_{Cy}. \tag{3}$$

In Mode 1 (1) V_{Cx}, V_{Cy} is the voltage across capacitors C_x, C_y, whereas V_{Lx}, V_{Ly}, and V_{Lz} are the voltages across inductors L_x, L_y, and L_z, correspondingly.

3.2. Mode 2 ($t_1 - t_2$). At mode 2, 3 inductors are attained following current path when these inductors are magnetized: I_{Lx} with source voltage (V_s) charges the C_x and follows the path V_s, V_{Lx}, D_x, C_x,and V_s. I_{Ly} and C_x charge to capacitor

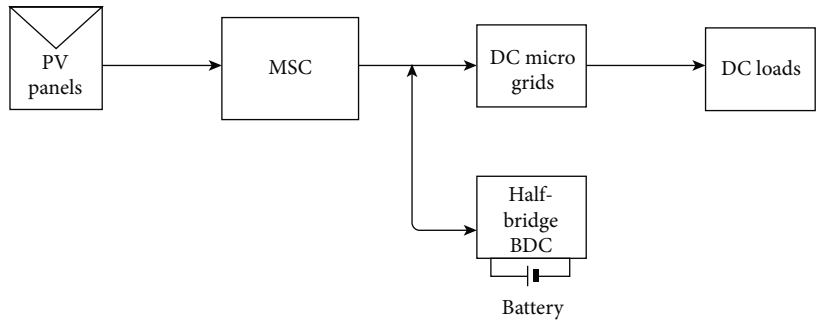

Figure 4: Proposed MSC integrated with PV system-based DC microgrid.

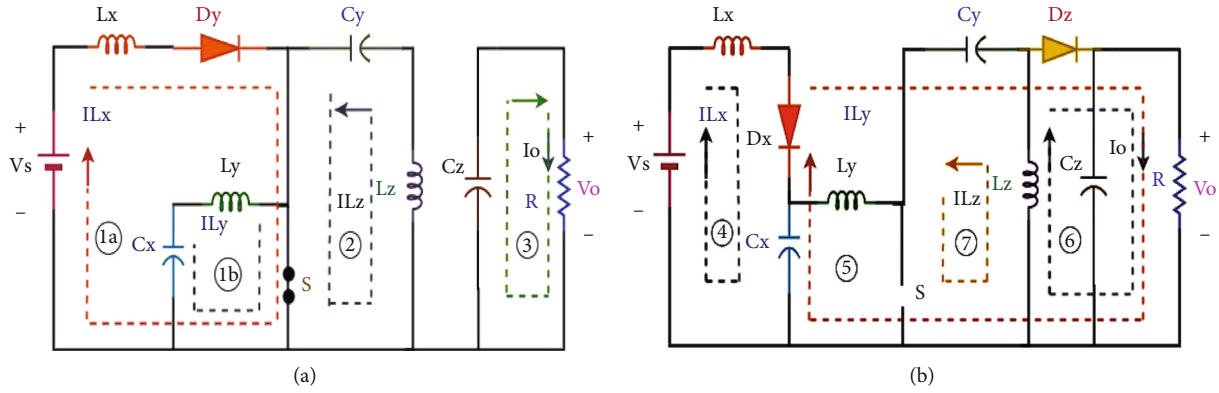

Figure 5: MSC operated at (a) mode1 (b) mode 2.

C_y as flows from VC_x, V_{Ly}, V_{Cy}, D_z, V_o and VC_x. Succeeding inductor I_{Lz} discharges over the DC load follows the path V_{Lz}, D_z, V_o shown in Figure 5(b).

$$\begin{aligned} V_{Lx} &= V_s - V_{Cx}, \\ V_{Ly} &= V_s - V_{Lx} - V_{Cy} - V_o, \\ V_{Ly} &= V_{Cx} - V_{Cy} - V_o, \\ V_{Lz} &= V_o. \end{aligned} \tag{4}$$

In mode 2, V_{Co} is the voltage across capacitor C_z. As per the volt second balance equation for the inductors L_1, L_2, and L_3,

$$\frac{V_{Cx}}{V_s} = \frac{1}{1-k}, \tag{5}$$

$$V_{Cy} = \left(\frac{V_{Cx}}{1-k}\right) - V_o, \tag{6}$$

$$\frac{V_o}{V_{Cx}} = \frac{k}{1-k}. \tag{7}$$

$$\text{Voltage gain } (M_{ccm}) = \frac{V_o}{V_s} = \frac{k}{(1-k)^2} \tag{8}$$

Using Equation (8) to analyze the voltage gain for the proposed converter is achieved by varying the duty ratio from 0.6 to 0.9 as follows. When K is 0.6, 0.7, 0.8, and 0.9, the corresponding voltage gains are 3.75, 7.78, 20, and 90. Hence, high voltage gain is obtained when the duty ratio is increased. From Table 2, only one controlled switch is enough to obtain the high gain in voltage with low voltage stress relating to the other converters. Due to more voltage gain of the proposed MSC, it can be preferable for DC microgrid applications.

4. Half-Bridge BDC

Nonisolated BDCs are essentially understood by the addition of a diode and an antiparallel diode to the switch of the unidirectional converter connected with a controllable power switch. Basically, buck, boost, buck-boost, SEPIC, and CUK DC-DC converters make some nonisolated BDCs when the diode in the above DC-DC converters is interchanged with a controllable power switch. Based on the voltage boosting methods, nonisolated BDCs whereas interleaved multilevel, switched capacitor, etc., Table 3 shows that half-bridge configuration type nonisolated BDCs are the most capable, high-proficient, and robust in configuration, and also, these BDCs give the high voltage gain compared with the other nonisolated BDCs.

Commonly, this BDC can work in both synchronous boost and buck modes for power flow in both forward and reverse directions. The working operation of the converter is described in 2 modes. When power switch P is turned

Table 2: Contrast among MSC with conventional nonisolated high gain DC-DC converter topologies.

Topologies	No. of element requirement			
	Capacitors	Diodes	Inductors	Switches
Switched capacitor-based active network converter	3	3	2	2
New hybrid boosting converter	3	3	1	1
Transformerless high gain boost converter	3	3	2	2
Quadratic boost converter	2	3	2	1
Modified SEPIC converter	**3**	**3**	**3**	**1**

Table 3: Evaluation of the half-bridge BDC with conventional nonisolated BDCs [6].

Topology in bidirectional DC-DC converters	Voltage conversion ratio in buck mode	Voltage conversion ratio in boost mode	Number of switches	Number of passive components
Half-bridge	D	$\frac{1}{1-D}$	2	3
Inverting bidirectional	$-\frac{D}{1-D}$	$-\frac{D}{1-D}$	2	3
CUK	$-\frac{D}{1-D}$	$-\frac{D}{1-D}$	2	5
SEPIC	$\frac{D}{1-D}$	$\frac{D}{1-D}$	2	5

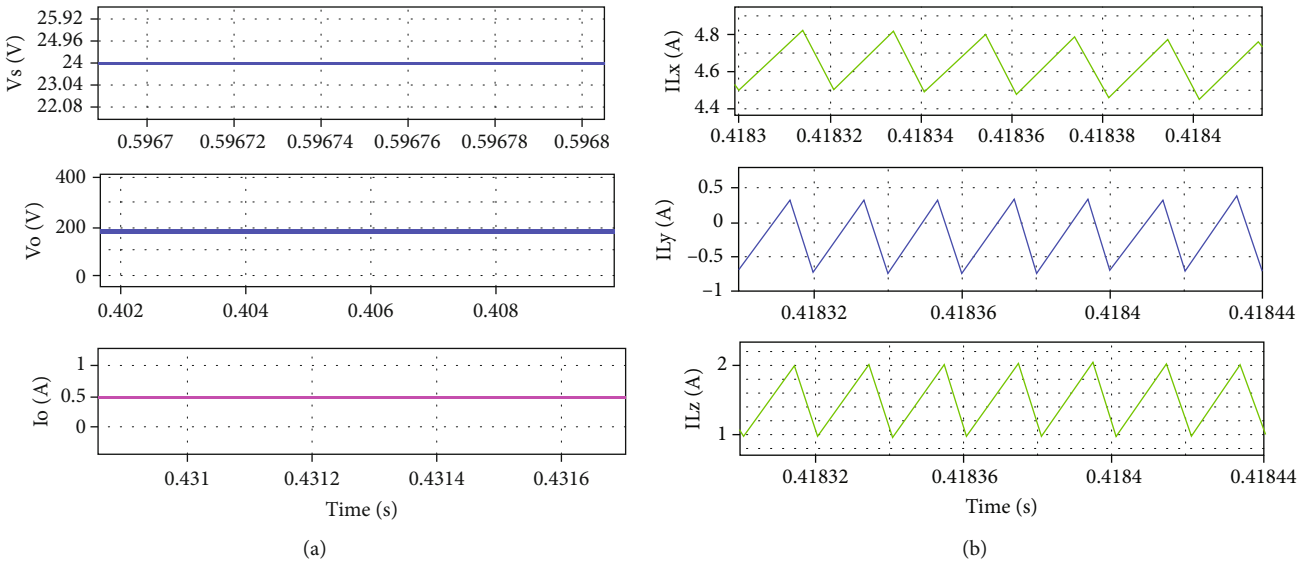

Figure 6: (a) DC supply, output voltage, and output current I_o and (b) inductor currents I_{Lx}, I_{Ly}, I_{Lz} of MSC.

on with the help of a required duty ratio control, the operation of this BDC is viewed in a forward step-down mode. When Q is turned on, then P is turned off with the help of a proper controlling duty ratio, this BDC can undergo a backward step-up operation as shown in Figure 3.

This BDC requires only two switches with three passive elements (one inductor and two capacitors). While comparing this BDC with conventional BDCs, this BDC has wide voltage gain; especially in boost mode, the cost of this BDC is less, and also, this BDC generates continuous output current without ripples. Generally, this converter operates in two modes, buck mode and boost mode.

Table 4: Performance parameters.

Parameters	Values
Input voltage	24 V
Power	100 W
Inductors	1 mH
Capacitors	220uF
Switching frequency	50,000 Hz
Duty ratio	0.7
Input current	4A

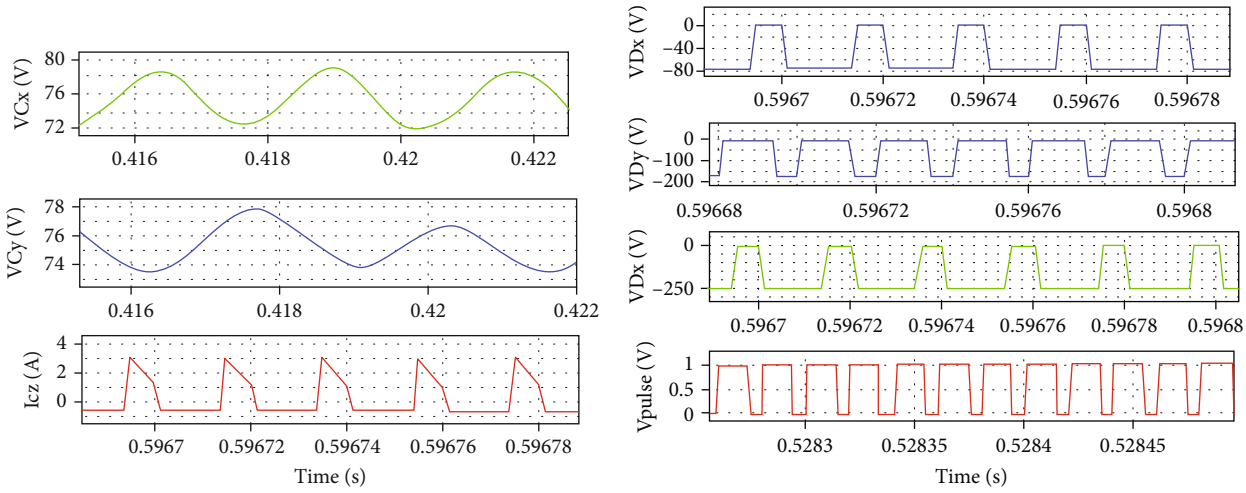

FIGURE 7: (a) Voltage across the capacitor V_{Cx},V_{Cy}, and current I_{Cz} and (b) voltage across D_x, D_y, D_z, and switching pulses of MSC.

5. Simulation Results and Discussion

Figure 6 shows the two input sources such as PV source and battery with half bridge BDC; here, the DC microgrid consists of DC loads. These blocks are connected to the MSC. MSC probably produces an effective DC voltage and current to the DC loads in DC microgrids from the PV source. If in case partially shaded conditions happened, PV panels do not supply the voltage required by the DC microgrid. For backup protection and to balance the supply voltage and currents with load voltage and currents, BDC with battery is required. Here, half-bridge BDC is used to supply voltage to the DC loads if in case PV does not satisfy the amount of voltage required by the DC loads.

5.1. Simulation Results of the MSC. Generally, MSC can produce wide voltage gain with continuous output current. Moreover, this MSC always uses the resources at the maximum level. It extensively produces the voltage gain with better efficiency. Usually, it is effectively operated by a fixed frequency and variable duty along with the PWM technique to generate a gate voltage to the power switch. The proposed MSC is successfully simulated in PSIM software and generates the output voltage at a higher voltage gain with the preferred output current required by the DC load. Here, this MSC, PSIM results are obtained without producing ripple content in its output voltage and current. Hence, it is well suited for DC microgrids and PV system applications. But conventional nonisolated DC-DC converters produce ripples in the percentage of 0.1%-0.5%. But MSC produces ripple content in the percentage of around 0.016. This ripple voltage is a negligible value. Therefore, it effectively produces output voltage without producing any ripple content in output voltage and current. The values of the passive and active parameters used in this entire project are viewed in Table 4.

Figure 6(a) describes the supply voltage, output voltage, and current of MSC as 24 V, 186.3 V, and 0.5A, respectively. These three waveforms are periodically DC in nature. Here,

TABLE 5: Evaluation of the simulation results of the MSC.

Parameters	Values
Supply voltage V_s	24 V
Output voltage V_o	186.3 V
Output current I_o	0.5A
Inductor currents I_{Lx}, I_{Ly}, and I_{Lz}	4.2A, 1.4A, and 0.5A
Capacitor voltages V_{Cx} and V_{Cy}	78.71 V, 76.75 V
I_{Cz} current flowing in the capacitor C_z	0.5A
Diode currents I_{Dx}, I_{Dy}, and I_{Dz}	76 V, 172 V, and 184 V
Voltage gain M_{ccm}	7.7
Supply frequency f_s	50 kHz

MSC cannot generate any ripple content in the output voltage and current. Thus, MSC always generates continuous current to the DC loads. Figure 6(b) shows that inductor L_x, L_y, and L_z current regarding the MSC with values of 4.2 A, 1.4 A, and 0.5 A (average) current, respectively. In mode I, currents flowing in three inductors are increasing with a positive slope and vice versa in mode II operation.

Figure 7(a) illustrates the capacitor voltages V_{Cx} and V_{Cy} , and the corresponding values are 78.71 V and 76.75 V. It is examined that approximately +80 V is obtained across the capacitors C_x and C_y. It is analyzed that the characteristic waveforms and this simulation results of capacitor voltages V_{C1} and V_{C2} are matched and steady state in nature (Figure 7(a)), current flowing in the capacitor C_z with the value of 0.5A (average value). The average current of this capacitor is exactly equal to the output current flowing in the resistor R. Figure 7(b) elaborates the diodes D_x, D_y, and D_z blocking voltages in reverse bias condition. During mode 1, diodes D_x and D_z are in forward bias condition, and these diodes generate peak inverse voltages similar to the capacitors C_x and C_z, and the corresponding values are

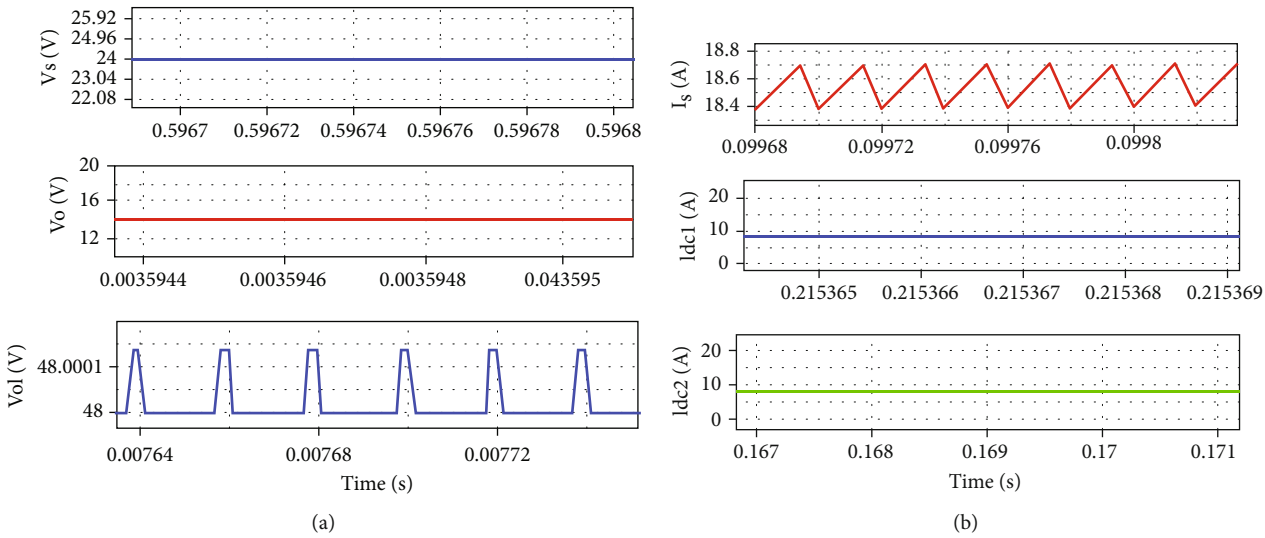

FIGURE 8: (a) DC supply V_s, output voltage V_o and V_{o1} half-bridge BDC in buck mode and (b) current I_s,I_{dc1}, and I_{dc2} of the PV system-based DC microgrid operated with half-bridge BDC in buck mode.

76 V and 184 V. It is shown in Table 5 that during mode 2 operation, peak inverse voltage is the same as the output voltage (V_o) around 186.3 V, which is obtained when diode D_y is under reverse bias condition. Figure 7(b) also shows the switching pulse voltage V_{pulse} of the MSC. Generally, every DC-DC converter is taking pulse voltage from the pulse generator based on its duty ratio control. Here, MSC's power switch also takes pulse voltage from the pulse generator with 70% duty ratio.

5.2. Simulation Results of the Half-Bridge BDC. Here,V_s is a supply voltage, andV_o and V_{o1} are the output voltages of a half-bridge BDC operated in buck or boost modes with the following values: V_s is 24 V and V_o and V_{o1} are 20 V and 48 V, which are shown in Figure 8(a). Based on the output voltages produced, the results are proving the feasibility of this BDC, which is effectively well integrated to the DC microgrids and feeds DC voltage to the DC loads in a reliable manner. Here, half-bridge BDC is operated in two modes. The first mode is a buck mode; in this mode, this BDC generates the output voltage V_o with the value of 20 V (average value). The second mode is a boost mode; in this mode, this BDC generates an output voltage V_{o1} with the value of 48 V. The output voltages of this BDC are determined by the duty ratio of 50%.

5.3. Simulation Results of the PV System-Based DC Microgrid Operated with Half-Bridge BDC in Buck Mode. Operation of the PV system-based DC microgrid with half-bridge BDC in buck mode, one can easily achieve the load demand with the help of the PV system with MSC. Here, V_s is a supply voltage of 24 V. And I_s is the supply or input current with 18.6 A. And this supply current is effectively satisfying the three DC load currents; I_{dc1} is 8.1 A, I_{dc2} is 8.1 A, and I_{buck} is 2.4 A. So, here, $I_s = I_{dc1} + I_{dc2} + I_{buck}$. And V_{dcbus} DC bus voltage across the DC microgrid is 183.5 V when MSC is simply triggered with a duty ratio of 0.7. Here, V_{dc1}, V_{dc2}, and V_{buck} are the DC voltages across the three DC loads with values of 12 V, 24 V, and 24 V. But here, the half-bridge BDC simply operated in a buck mode can act as a third DC load. Moreover, this DC load will always be supplied by the input resource called the PV system. Here, calculate the supply current ripple $I_{s\,ripple}$ of the PV system-based DC microgrid operated with half-bridge BDC in buck mode,

$$I_{s\,ripple} = \frac{(I_{s\ max} - I_{s\ min})}{I_{s\,avg}},$$
$$I_{s\,ripple} = 0.0056\ \text{A}. \tag{9}$$

Here, the negligible ripple in supply current I_s of the PV system-based DC microgrid operated with half-bridge BDC in buck mode. At this stage, the whole system is effectively satisfied with all three DC loads. Thus, effective supply voltage and current can reach the three DC loads in an effective manner. Figure 8 shows the DC currents I_{dc1}, I_{dc2} flowing in the half-bridge BDC in buck mode of the PV system-based DC microgrid operated with half-bridge BDC. During buck mode, obtained current values are 7.55 A and 7.3 A.

Figure 9 shows that current flowing I_{buck}, dc bus voltage V_{dc_bus}, DC voltages V_{dc1}, V_{dc2}, and voltage of the half-bridge BDC in buck mode V_{buck} of the PV system-based DC microgrid operated with half-bridge BDC in buck mode with the values of 3.1 A,183.5, 12 V, 24 V. Here, these three voltages are appearing as an output voltage of the DC load ends which are connected to the DC microgrid. Calculated dc bus voltage ripple $V_{dc\_bus\_ripple}$ of a of the PV system-based DC microgrid operated with half-bridge BDC in buck mode. Equation (11) shows that negligible voltage ripple occurred in dc bus voltage V_{dc_bus} be noticed that with the help of MSC, the PV system effectively serves the dc loads which are connected in a DC microgrid without generating

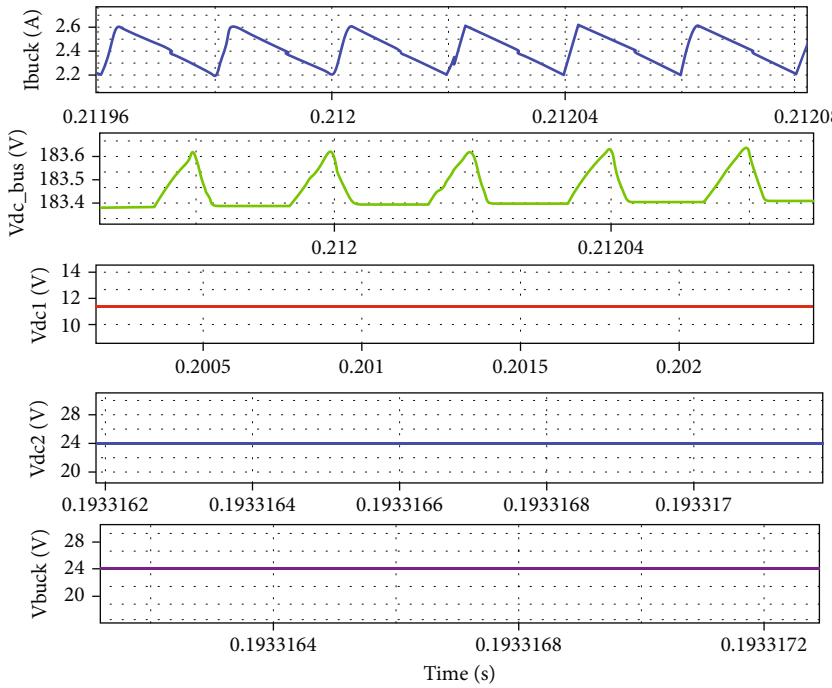

FIGURE 9: I_{buck}, DC bus voltage V_{dc_bus}, V_{dc1}, V_{dc2}, and buck voltage V_{buck} of the PV system-based DC microgrid operated with half-bridge BDC in buck mode.

any current or voltage ripples in the mode of the PV system-based DC microgrid operated with half-bridge BDC in buck mode. The input power P_{in} supplied by the PV system with the help of the MSC effectively satisfy all three dc loads' output power P_{out} connected in DC microgrid. In this mode, 12 V to 24 V DC loads effectively utilized the output power produced from the integration of the PV system with MSC, and the parameters are given in Table 6.

$$V_{dc\_bus\,ripple} = \frac{(V_{dc\_bus\_max} - V_{dc\_bus\_min})}{V_{dc\_bus\_avg}}, \tag{10}$$

$$V_{dc\_bus\,ripple} = 0.00042, \tag{11}$$

$$P_{in} > P_{out}, \tag{12}$$

$$V_{in}I_{in} > V_{out}I_{out}, \tag{13}$$

$$V_sI_s > V_{dc1}I_{dc1} + V_{dc2}I_{dc2} + V_{buck}I_{buck}. \tag{14}$$

From Table 4, three substituting values of the parameters specified in Equation (14) are

$$\begin{aligned} V_sI_s &= 428.4\ W, \\ V_{dc1}I_{dc1} + V_{dc2}I_{dc2} + V_{buck}I_{buck} &= 340.2\ W. \end{aligned} \tag{15}$$

By means of the numerical analysis, this PV system-based DC microgrid operated with half-bridge BDC in buck mode with the application of MSC can generate the input power more than the load requirement without generating any fluctuations in output power.

TABLE 6: Parameters of PV system-based DC microgrid operated with half-bridge BDC in buck mode.

Parameters	Values
Supply voltage V_s	24 V
DC bus voltage V_{dc_bus}	183.5 V
Voltage of the half-bridge BDC in buck mode V_{buck}	24 V
DC voltage for the DC load 1 V_{dc1}	12 V
DC voltage for the DC load 2 V_{dc2}	24 V
Supply current I_s	18.6 A
Current flowing in the half-bridge BDC in buck mode I_{buck}	2.4 A
DC for the DC load 1 I_{dc1}	8.1 A
DC for the DC load 2 I_{dc2}	8.1 A

5.4. Simulation Results of the PV System-Based DC Microgrid Operated with Half-Bridge BDC in Boost Mode. In this operation of the PV system-based DC microgrid operated with half-bridge BDC in boost mode, one can easily achieve the load demand with the help of the PV system and half-bridge BDC operated in boost mode with MSC. Here, V_{s1} and V_{boost} are supply voltages with the value of 24 V and 40 V. And I_{s1} and I_{boost} are supply or input currents with values of 2.4 A and 16.6 A. These supply currents are effectively satisfying the two DC load currents; I_{dc4} is 8.4 A, and I_{dc5} is 8.2 A. Therefore, $I_{s1} + I_{boost} \geq I_{dc3} + I_{dc4}$ and V_{dc_bus} DC bus voltage across the DC microgrid with 183.76 V when MSC is simply triggered with a duty ratio

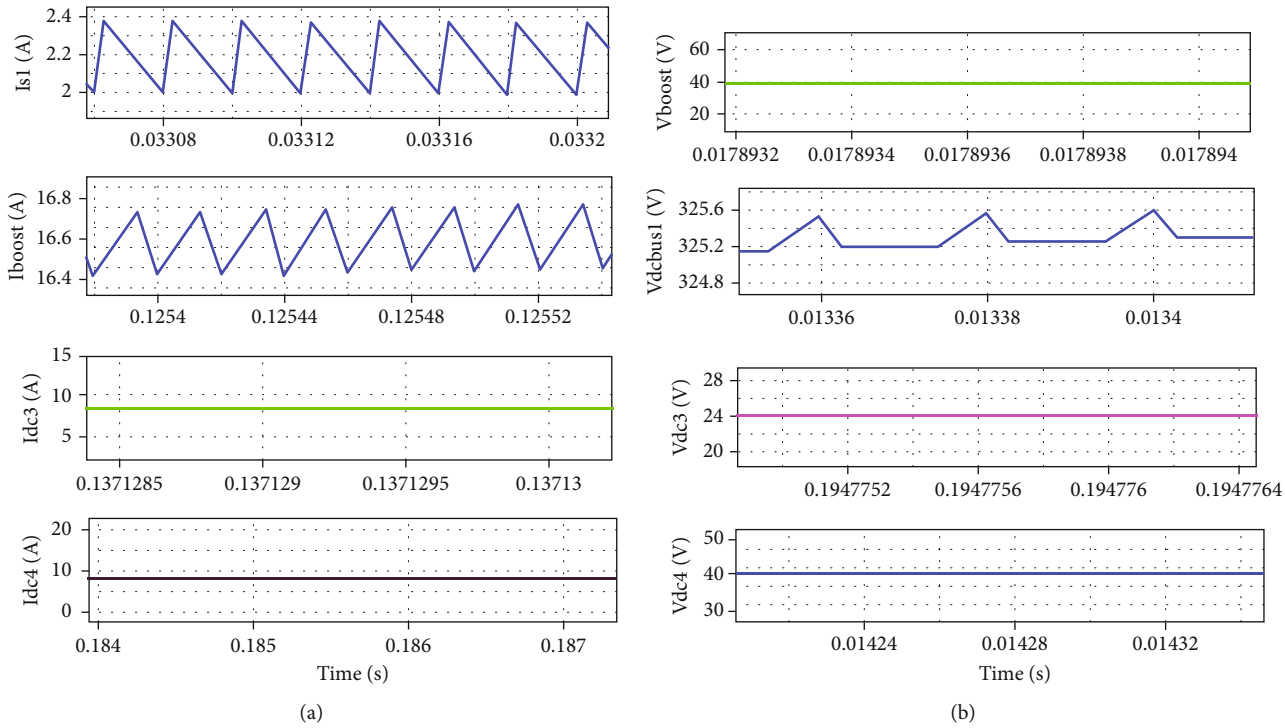

FIGURE 10: (a) DC supply current I_{s1},I_{boost},I_{dc3}, and I_{dc4} and (b) DC boost voltage V_{boost} and bus voltage $V_{\text{dc\_bus1}}$ and dc voltage V_{dc3} and V_{dc4} of the PV system-based DC microgrid operated with half-bridge BDC in boost mode.

of 0.7. Here, V_{dc4} and V_{dc5} are the DC voltages across the three DC loads with values of 12 V and 24 V. But half-bridge BDC simply operated in a boost mode can act as a supply system with a battery source. Moreover, these DC loads are always supplied by the input resources called by the PV system and battery with half-bridge BDC operated in boost mode.

Figure 10(a) shows that dc supply currents I_{s1} and current flowing in the half-bridge BDC in boost mode I_{boost} of the PV system-based DC microgrid operated with half-bridge BDC in boost mode with the values of 3.4 A and 23 A. These two currents are supply currents to the PV system-based DC microgrid operated with half-bridge BDC in boost mode.

Here, the calculated current ripple $I_{\text{boost\_ripple}}$ of the half-bridge BDC in boost mode is given as

$$I_{\text{boost\_ripple}} = \frac{(I_{\text{boost\_max}} - I_{\text{boost\_min}})}{I_{\text{boost\_avg}}},$$
$$I_{\text{boost\_ripple}} = 0.034. \tag{16}$$

Here, the negligible ripple in current I_{boost} is achieved by the PV system-based DC microgrid operated with half-bridge BDC in boost mode. At this juncture, the whole system effectively satisfied all two DC loads. As a result, this effective supply voltage and current can reach the three DC loads effectively. Figure 10(a) also shows that DC, I_{dc3} and I_{dc4}, of the PV system-based DC microgrid operated with half-bridge BDC in boost mode with the values of 13.2 A and 13.2 A. Here, these two currents are feeding the dc loads. Figure 10(b) shows the voltage of the half-bridge BDC in boost mode V_{boost} of the PV system-based DC microgrid operated with half-bridge BDC in boost mode with the value of 40 V when the supply voltage is given as24 V. Here, these two voltages are appearing as supply voltages of the PV system-based DC microgrid operated with half-bridge BDC in boost mode. Here, the calculated dc bus voltage ripple $V_{dc\_bus1\_ripple}$ of the PV system-based DC microgrid operated with half-

TABLE 7: Parameters of the PV system-based DC microgrid operated with half-bridge BDC in boost mode.

Parameters	Values
Supply voltage V_{s1}	24 V
DC bus voltage $V_{\text{dc\_bus1}}$	325.2 V
Voltage of the half-bridge BDC in boost mode V_{boost}	40 V
DC voltage for the DC load 3 V_{dc3}	24 V
DC voltage for the DC load 4 V_{dc4}	48 V
Supply current I_{s1}	2.4 A
Current flowing in the half-bridge BDC in boost mode I_{boost}	16.6 A
DC for the DC load 3 I_{dc3}	9.5 A
DC for the DC load 4 I_{dc4}	9.5 A

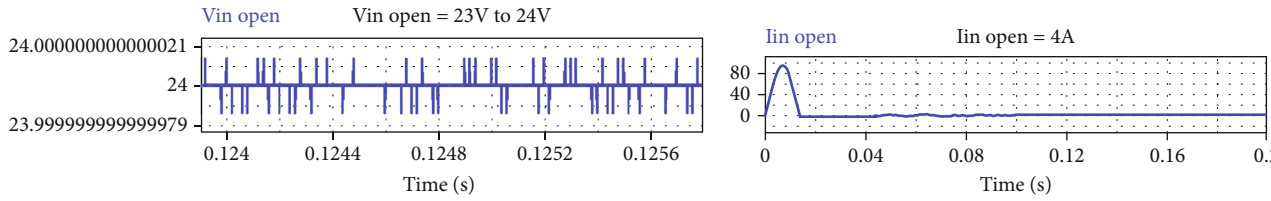

FIGURE 11: (a) Input voltage $V_{\text{in open}}$. (b) Input current $I_{\text{in open}}$.

bridge BDC in boost mode.

$$V_{\text{dc\_bus1\_ripple}} = \frac{(V_{\text{dc\_bus1\_max}} - V_{\text{dc\_bus1\_min}})}{V_{\text{dc\_bus1\_avg}}}, \tag{17}$$

$$V_{\text{dc\_bus1\_ripple}} = 0.00065. \tag{18}$$

From Equation (18), the negligible ripple in dc bus voltage $V_{\text{dc\_bus}}$ is obtained from the PV system-based DC microgrid operated with half-bridge BDC in boost mode. Therefore, the whole system effectively satisfied all two DC loads. Hence, supply voltage and current can reach the two DC loads effectively.

Figure 10(b) also shows that dc voltages V_{dc3} and V_{dc4} of the PV system-based DC microgrid operated with half-bridge BDC in boost mode with the values of 24 V and 48 V. Here, these two voltages are appearing as an output voltage to the dc loads which are connected DC microgrids. Here, one thing to notice is that with the help of MSC, a PV system and energy storage element connected with the help of a half-bridge BDC can effectively serve the dc loads which are connected in a DC microgrid without generating any current or voltage ripples in the mode of the PV system-based DC microgrid operated with half-bridge BDC in boost mode. The input power P_{in} supplied by the PV system and energy storage element connected with the help of a half-bridge BDC with the help of the MSC effectively satisfy the two dc loads output power P_{out} connected in DC microgrid in this PV system-based DC microgrid operated with half-bridge BDC in boost mode. In this mode, 24 V to 48 V DC loads effectively utilized the output power produced from the integration of the PV system with MSC, and parameters are described in Table 7.

Neglecting the losses (switch and diode power losses),

$$\begin{aligned} P_{\text{in}} &> P_{\text{out}}, \\ V_{\text{in}} I_{\text{in}} &> V_{\text{out}} I_{\text{out}}, \\ V_s I_s + V_{\text{boost}} I_{\text{boost}} &> V_{\text{dc3}} I_{\text{dc3}} + V_{\text{dc4}} I_{\text{dc4}}. \end{aligned} \tag{19}$$

From Table 5, the substituting values of the parameters specified in the above equation are

$$\begin{aligned} V_s I_s + V_{\text{boost}} I_{\text{boost}} &= 721.6\ W, \\ V_{\text{dc3}} I_{\text{dc3}} + V_{\text{dc4}} I_{\text{dc4}} &= 684\ W. \end{aligned} \tag{20}$$

Based on the numerical analysis, this PV system-based DC microgrid operated with half-bridge BDC in boost mode with the application of MSC can generate the input power more than the load requirement without generating any fluctuations in output power. This entire paper elaborated about the implementation of a modified SEPIC converter with DC microgrids for effectively satisfying the DC loads in an efficient manner. Moreover, this converter can effectively operate with PV system to obtain the maximum voltage gain. Here, input voltage with disturbances is feed to the MSC. And then output voltage of MSC is producing some transients in its output voltage waveform. Here, performance parameters under time domain specifications are evaluated for the open loop control of MSC's output voltage.

5.5. Dynamic Response of the System against the Environmental Conditions. This section describes the overall performance of the system against all environmental conditions. The research scholars know that the PV system voltage is varying with respect to any climate Conditions (1). To eradicate this problem with the help of the proposed MSC, the proposed MSC can produce constant output voltage when it takes varying input voltage also. The reason behind this is that the proposed MSC can effectively utilize the input resources in a greater way [20]. So, the following PSIM simulation-based results are evident for the proposed MSC which effectively has a good dynamic response regarding the control of DC microgrid loads. Figures 11(a) and 11(b) prompt the input current and voltage waveforms of the open loop control of MSC. Here, input current is 4 A, and the input voltage is 24 V of the open loop control of MSC. These waveforms regarding the open loop control of MSC are having some disturbances. Then, these input currents and voltage are fed to MSC, and finally, output voltage and current of open loop MSC are viewed at DC loads driven by MSC.

Figure 12 can illustrate the open loop MSC's output voltage waveform, damping ratio (θ), undamped natural frequency (ω_n), and damped natural frequency (ω_d) parameters are calculated with the help of the logarithmic decrement method [25]. Damping ratio $(\theta) = 0.5$, undamped natural frequency $(\omega_n) = 1.2\ rad/\text{sec}$, damped natural frequency $\omega_{\text{d}} = \omega_{\text{n}}\sqrt{1-\theta^2} = 1.03$ rad/sec, and here, $\beta = \cos^{-1}\theta$.

The mathematical calculations described in Table 8 demonstrate that the peak overshoot value is 6.30%, delay time, peak time, and rise time are at less than 3 sec, and

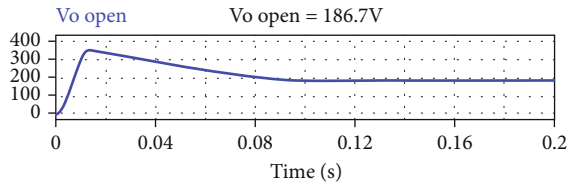

Figure 12: Output voltage $V_{o\,open}$.

Table 8: Evaluation of performance parameters of the output voltage of the open loop control of MSC.

Performance parameters	Formulae	Values
Delay time (T_d)	$T_d = \frac{1+0.7\theta}{\omega_n}$	1.12 sec
Rise time (T_r)	$T_r = \frac{\pi-\beta}{\omega_d}$	3.03 sec
Peak time (T_p)	$T_p = \frac{\pi}{\omega_d}$	5.04 sec
Peak overshoot (%M_p)	$\%M_p = 100e^{-\pi\theta/\sqrt{1-\theta^2}}$	6.30%
Settling time (T_s)	$T_s = \frac{4}{\theta\omega_n}$	4.67 sec

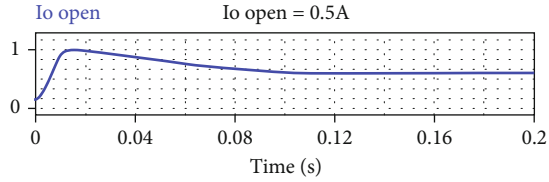

Figure 13: Output current $I_{o\ open}$.

finally, the settling time is at 4.67 sec regarding the output voltage of the open loop control of MSC. If MSC's output voltage can be controlled, the output voltage of this MSC definitely produces no transients and has a peak overshoot nearly at 6%, and the settling time of this output voltage waveform is nearly at 5 sec. So, these values prove that open loop control of MSC can generate constant DC output voltage in the period of less than 0.1 sec in Figure 13. So, that is the reason closed-loop control of MSC is implemented to generate a constant output voltage and current for DC microgrid loads driven by MSC.

6. Conclusion

The MSC topology for PV system-based DC microgrids is discussed and simulated using PSIM software. The advantages of using MSC topology are addressed. PV system with an MSC configuration continuously generates output current without producing any ripples. This configuration gives the output voltage with high gain, delivers the required amount of power supply demanded by the DC loads, and achieves a reliable power supply to the DC loads by using the integration of an MSC-based PV system. And the dynamic response of the overall system is also presented, especially this topology which is well suited for domestic applications. Nowadays, most of the houses are equipped with DC LED lamps, BLDC motor-based ceiling fans, etc. These applications require DC supply. Domestic appliances which are operated by the DC supply definitely satisfy their load demand when they are using the topology addressed in the proposed work.

Data Availability

Data sharing is not applicable to this article as no datasets were generated or analyzed during the current study.

Conflicts of Interest

The authors declare that they have no conflicts of interest.

References

[1] U. Shahzad, "The need for renewable energy sources," *International Journal of Information Technology and Electrical Engineering*, vol. 2, 2017.

[2] E. Mclamb, "Fossil fuels vs. renewable energy resources," 2011, [Accessed 20th April 2015], http://www.ecology.com/2011/09/06/fossil-fuelsrenewable-energy-resources/.

[3] C. J. Anders, "Greatest fossil fuels disasters in human history," 2010, [Accessed 20th April 2015], http://io9.com/5526826/greatest-fossil-fuel-disasters-inhuman-history.

[4] D. Kumar, F. Zare, and A. Ghosh, "DC Microgrid technology: system architectures, AC grid interfaces, grounding schemes, power quality, communication networks, applications, and standardizations aspects," *IEEE Access*, vol. 5, article 12230, 2017.

[5] T. Dragičević, X. Lu, J. C. Vasquez, and J. M. Guerrero, "DC microgrids—part i: a review of control strategies and stabilization techniques," *IEEE Transactions on Power Electronics*, vol. 31, no. 7, pp. 4876–4891, 2016.

[6] N. Yang, B. Nahid-Mobarakeh, F. Gao, D. Paire, A. Miraoui, and W. Liu, "Modeling and stability analysis of multi-time scale DC microgrid," *Electric Power Systems Research*, vol. 140, pp. 906–916, 2016.

[7] M. Nymand and M. A. E. Andersen, "High-efficiency isolated boost DC–DC converter for high-power low-voltage fuel-cell applications," *IEEE Transactions on Industrial Electronics*, vol. 57, no. 2, pp. 505–514, 2010.

[8] K. I. Hwu and W. Z. Jiang, "Isolated step-up converter based on flyback converter and charge pumps," *IET Power Electronics*, vol. 7, no. 9, pp. 2250–2257, 2014.

[9] S. B. Tank, K. Manavar, and N. Adroja, "Non-isolated bi-directional DCDC converters for plug-in hybrid electric vehicle charge station application," in *Proc. of Emerging Trends in Computer & Electrical Engineering (ETCEE 2015)*, pp. 13-14, Rajkot, India, April 2015.

[10] M. Lakshmi and S. Hemamalini, "Nonisolated high gain DC–DC converter for DC microgrids," *IEEE Transactions on Industrial Electronics*, vol. 65, no. 2, pp. 1205–1212, 2018.

[11] W. Li and X. He, "Review of nonisolated high-step-up DC/DC converters in photovoltaic grid-connected applications," *IEEE Transactions on Industrial Electronics*, vol. 58, no. 4, pp. 1239–1250, 2011.

[12] Y. Cao, V. Samavatian, K. Kaskani, and H. Eshraghi, "A novel nonisolated ultra-high-voltage-gain DC–DC converter with low voltage stress," *IEEE Transactions on Industrial Electronics*, vol. 64, no. 4, pp. 2809–2819, 2017.

[13] D. Yu, J. Yang, R. Xu, Z. Xia, H.-H. C. Iu, and T. Fernando, "A family of module-integrated high step-up converters with dual coupled inductors," *IEEE Access*, vol. 6, pp. 16256–16266, 2018.

[14] M. Zhang, Y. Xing, H. Wu, H. Hu, and X. Ma, "A dual coupled inductors-based high step-up/step-down bidirectional DC-DC converter for energy storage system," in *2017 IEEE Applied Power Electronics Conference and Exposition (APEC)*, pp. 2958–2963, Tampa, FL, USA, March 2017.

[15] M. Nilanjan and S. Dani, "Control of cascaded DC–DC converter-based hybrid battery energy storage systems—part I: stability issue," *IEEE Transactions on Industrial Electronics*, vol. 63, no. 4, pp. 2340–2349, 2016.

[16] J. C. Rosas-Caro, F. Mancilla-David, J. C. Mayo-Maldonado, J. M. Gonzalez-Lopez, H. L. Torres-Espinosa, and J. E. Valdez-Resendiz, "A transformer-less high-gain boost converter with input current ripple cancelation at a selectable duty cycle," *IEEE Transactions on Industrial Electronics*, vol. 60, no. 10, pp. 4492–4499, 2013.

[17] Y. Tang, T. Wang, and Y. He, "A switched-capacitor-based active-network converter with high voltage gain," *IEEE Transactions on Power Electronics*, vol. 29, no. 6, pp. 2959–2968, 2014.

[18] B. Wu, S. Li, Y. Liu, and K. M. Smedley, "A new hybrid boosting converter for renewable energy applications," *IEEE Transactions on Power Electronics*, vol. 31, no. 2, pp. 1203–1215, 2016.

[19] K. H. Beena and A. Benny, "Analysis and implementation of quadratic boost converter for nanogrid applications," *International Journal of Advanced Research in Electrical, Electronics and Instrumentation Engineering*, vol. 4, no. 7, pp. 6043–6048, 2015.

[20] P. K. Maroti, S. Padmanaban, J. B. Holm-Nielsen, M. S. Bhaskar, M. Meraj, and A. Iqbal, "A New Structure of High Voltage Gain SEPIC Converter for Renewable Energy Applications," vol. 7, 2019.

[21] T. Esram and P. L. Chapman, "Comparison of photovoltaic array maximum power point tracking techniques," *IEEE Transactions on Energy Conversion*, vol. 22, no. 2, pp. 439–449, 2007.

[22] G. de Cesare, D. Caputo, and A. Nascetti, "Maximum power point tracker for portable photovoltaic systems with resistive-like load," *Solar Energy*, vol. 80, no. 8, pp. 982–988, 2006.

[23] F. Caricchi, F. Crescimbini, G. Noia, and D. Pirolo, "Experimental study of a bidirectional DC-DC converter for the DC link voltage control and the regenerative braking in PM motor drives devoted to electrical vehicles," in *Proceedings of 1994 IEEE Applied Power Electronics Conference and Exposition - ASPEC'94*, pp. 381–386, Orlando, FL, USA, 1994.

[24] D. C. Denny and M. Shahin, "Analysis of bidirectional SEPIC/zeta converter with coupled inductor," in *2015 International Conference on Technological Advancements in Power and Energy (TAP Energy)*, pp. 103–108, Kollam, India, 2015.

[25] D. J. Inman, *Engineering Vibrations*, Pearson Education, Inc., 2007.